Circuit topology for synchronizing neurons in spontaneously active networks

Naoya Takahashi[a], Takuya Sasaki[a], Wataru Matsumoto[a], Norio Matsuki[a], and Yuji Ikegaya[a,b,1]

[a]Laboratory of Chemical Pharmacology, Graduate School of Pharmaceutical Sciences, University of Tokyo, Tokyo 113-0033, Japan; and [b]Precursory Research for Embryonic Science and Technology, Japan Science and Technology Agency, Kawaguchi 332-0012, Japan

Edited by Robert Desimone, Massachusetts Institute of Technology, Cambridge, MA, and approved April 15, 2010 (received for review December 19, 2009)

Spike synchronization underlies information processing and storage in the brain. But how can neurons synchronize in a noisy network? By exploiting a high-speed (500–2,000 fps) multineuron imaging technique and a large-scale synapse mapping method, we directly compared spontaneous activity patterns and anatomical connectivity in hippocampal CA3 networks ex vivo. As compared to unconnected pairs, synaptically coupled neurons shared more common presynaptic neurons, received more correlated excitatory synaptic inputs, and emitted synchronized spikes with approximately 10^7 times higher probability. Importantly, common presynaptic parents per se synchronized more than unshared upstream neurons. Consistent with this, dynamic-clamp stimulation revealed that common inputs alone could not account for the realistic degree of synchronization unless presynaptic spikes synchronized among common parents. On a macroscopic scale, network activity was coordinated by a power-law scaling of synchronization, which engaged varying sets of densely interwired (thus highly synchronized) neuron groups. Thus, locally coherent activity converges on specific cell assemblies, thereby yielding complex ensemble dynamics. These segmentally synchronized pulse packets may serve as information modules that flow in associatively parallel network channels.

action potential | calcium imaging | microcircuit | spontaneous activity | synchronization

Synchronized spikes prevail in cortical networks (1, 2). Their modulations are commonly found in relation to attention, sensory processing, and motor behaviors (3–8) and are implied in perceptual binding (9). From computational aspects, spike synchronization is crucial in information propagation (10, 11). As single synapses are weak and stochastic, spikes cannot propagate to a downstream network unless they synchronize. Moreover, synchronized spikes are known to induce long-lasting synaptic plasticity, depending on their relative timings between presynaptic and postsynaptic neurons (12, 13).

Spikes do not synchronize only between a pair of neurons but also among a set of neurons, often yielding high-order complex dynamics, as in cell assemblies (14–17), synfire chains (10, 18), and neuronal avalanches (19). The complex dynamics usually emerge through autoassociative recurrent networks in which neurons are sparsely interconnected to constitute relatively small groups. Thus, a neural correlation can report a local network state (20–22).

Independent studies have addressed the topology underlying either "functional" (synchronous) or "anatomical" (synaptic) connectivity among multiple neurons (23–34), but very little is known about their relationship. In this work, we used high-speed functional multineuron calcium imaging (fMCI), large-scale synapse mapping, and multiple whole-cell and dynamic patch-clamp recording techniques and directly compared spatiotemporal spike patterns with synaptic wiring architectures. We report that CA3 networks ex vivo are nonrandomly woven to facilitate local spike synchronization under globally coherent inhibitory backgrounds.

Results

Strong Spike Synchronization Between Synaptically Connected Neurons. In rat entorhino-hippocampal slice cultures, 104 pairs of adjacent CA3 pyramidal cells (PCs) were randomly selected for whole-cell recordings (Fig. 1*A*). The connectivity density among CA3 PCs was 28.8%. This connection ratio is higher than the connectivity (2–8%) reported in acute slice preparations (35, 36). In acute hippocampal slices, 75% to 90% of the axons of CA3 pyramidal neurons are amputated even in 500-μm-thick slices (37). Therefore, organotypically cultured ex vivo networks are likely to self-restore their complexity to a realistic extent. In support of this, we found that neither levels nor patterns of spontaneous excitatory postsynaptic currents (sEPSCs) or inhibitory postsynaptic currents (sIPSCs) differed between ex vivo and in vivo hippocampal neurons (Fig. S1). As the ex vivo recovery of slice cultures occurs without external inputs (unlike normal development), this work will describe the "default" network dynamics that emerge under disturbance-free conditions.

Of 104 PC pairs, we encountered 16 bidirectionally connected pairs. Given the connection probability p and the total number of pairs N, the statistically expected number of bidirectional pairs would be Np^2, i.e., 8.6 pairs. In our datasets, therefore, the number of bidirectionally connected pairs was 1.9 times higher than expected ($P = 0.012$) (30), suggesting that CA3 recurrent networks are topologically biased to enhance local connectivity.

When the neuron pairs were held in current-clamp mode, we sometimes found spontaneous spikes synchronized (Fig. 1*B*). To quantify the synchrony level, we introduce the scalar measure S, based on statistical salience of the observed number of synchronized spikes relative to chance. Specifically, we counted all synchronized spikes, i.e., any pairs of spikes that concurred in two neurons within a given time lag. If neuron$_i$ and neuron$_j$ are independent units that fire in a random manner, the probability $P(n)$ that they exhibit n synchronized spikes during the observation period t is given by the Poisson equation:

$$P_{i,j}(n) = \frac{m_{i,j}^n}{n!} e^{-m_{i,j}} \quad [1]$$

where $m_{i,j}$ is the expected number of synchronized spikes, i.e., $f_i \times f_j \times t$, and f_i and f_j denote the spike rates of neuron$_i$ and neuron$_j$, respectively. When spikes synchronize n times, the probability $\bar{P}_{i,j}$ (rareness) is given as follows:

$$\bar{P}_{i,j} = \sum_{k=n}^{\infty} P_{i,j}(k) = 1 - \sum_{k=0}^{n-1} P_{i,j}(k) \quad [2]$$

Then, we defined the surprise index ($S_{i,j}$) as $-\log_2 \bar{P}_{i,j}$ (38).

Author contributions: N.T., N.M., and Y.I. designed research; N.T. and T.S. performed research; N.T. and W.M. analyzed data; and N.T. and Y.I. wrote the paper.

The authors declare no conflict of interest.

[1]To whom correspondence should be addressed. E-mail: ikegaya@mol.f.u-tokyo.ac.jp.

This article contains supporting information online at www.pnas.org/lookup/suppl/doi:10.1073/pnas.0914594107/-/DCSupplemental.

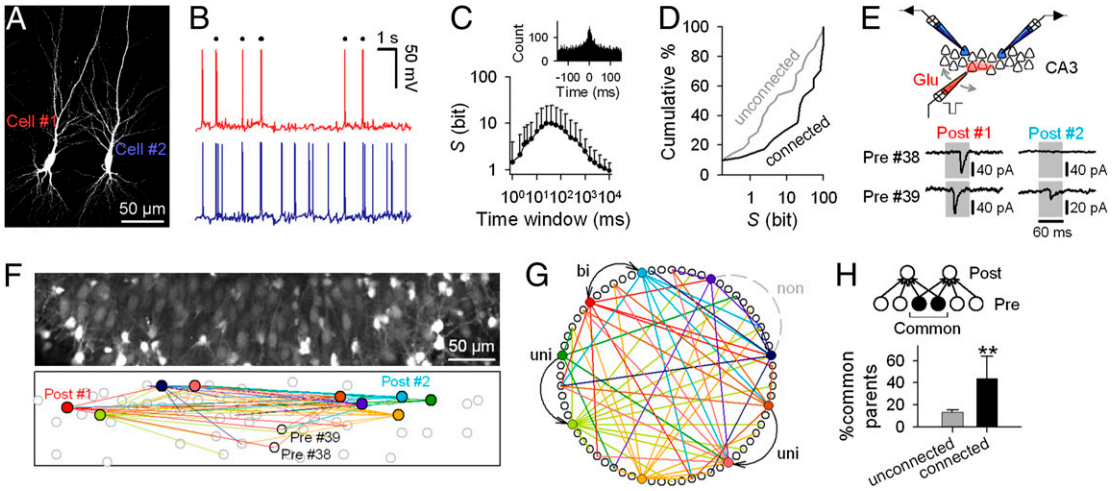

Fig. 1. Linkage of spike synchronization and synaptic connectivity. (*A*) Biocytin reconstruction of highly synchronized PCs. (*B*) Spontaneous activity exhibited by the neuron pairs shown in *A*. Dots indicate synchronized spike pairs. (*C*) (*Upper*) Cross-correlation histogram showing the spike-triggered distribution of spikes emitted by another neuron (n = 56 pairs). (*Lower*) S peaked at time windows of 10 to 50 ms (n = 39 pairs). (*D*) Synaptically connected pairs displayed significantly higher S than unconnected pairs (P = 0.032, Kolmogorov-Smirnov test). Data of unidirectional and bidirectional pairs were mixed, as there was no statistical difference ($P > 0.1$). (*E*) Diagram of ROTing for synapse mapping. (*Upper*) Two postsynaptic neurons were voltage-clamped (blue), and their presynaptic neurons were searched based on timings between EPSCs in the patched neurons and glutamate-evoked presynaptic calcium events (red). (*Lower*) Representative synaptic responses found by ROTing. Postsynaptic synaptic currents were aligned at presynaptic calcium spike timings (60-ms jitters allowed; gray). Presynaptic cell 38 projected to postsynaptic cell 1, whereas cell 39 projected to cells 1 and 2. The locations of these cells are shown in *F*. (*F*) Representative synaptic connectivity, in which 63 connections were identified to project to nine patched neurons (color-filled circles). Color lines indicate synaptic links to the correspondingly colored neurons. (*G*) Cells in *E* are circularly arranged. Arrows outside the circle indicate unidirectional (uni) or bidirectional (bi) synaptic connections between simultaneously patched neurons. (*H*) Synaptically coupled neuron pairs were innervated by larger proportions of common presynaptic neurons, compared with unconnected pairs (**P = 0.0043, Mann-Whitney U test; n = 5 unconnected pair vs. eight connected pairs).

For extremely synchronized pairs with $S > 100$ bits, S is denoted as 100 bits to avoid arithmetic precision problems in computing floating-point numbers. Thus, S ranges between 0 and 100 bits, with higher S reporting stronger synchronization.

S varies as a function of time widows for synchrony detection. It peaked at time windows of 10 to 50 ms (Fig. 1*C*). In accord with this, cross-correlation histogram of spike timings in neuron pairs (Fig. 1*C Inset*) showed a peak at 0 ms with an SD of 25 ms (fitted to the Gaussian curve). We therefore selected the 10-ms bin in the following analysis, unless otherwise specified.

Synaptically connected pairs were more synchronized than uncoupled pairs (Fig. 1*D*); the mean S for synaptic pairs was higher by 24 bits than that for uncoupled pairs, indicating that, on average, synaptic pairs exhibited synchronized spikes with a 1.7×10^7 (i.e., 2^{24}) times higher probability. Consistent with this, the probability to find synaptic pairs increased with S (Fig. S2). Therefore, the functional and anatomical connectivity is reciprocally, if not perfectly, linked at the single-cell level.

Common Presynaptic Neurons Shared by Synaptically Connected Neurons. To probe the synaptic wiring pattern among CA3 PCs, we employed reverse optical trawling (ROTing), a new optical mapping method (39). While EPSCs were recorded simultaneously from two randomly selected PCs, a small number of nearby neurons were sequentially activated by iontophoretic application of glutamate through a glass pipette that was slowly moved to survey the surrounding network (Fig. 1*E*). Spikes of glutamate-activated neurons were captured as somatic Ca^{2+} transients with high-speed fMCI (Fig. S3). Neurons that exhibited calcium transients immediately before EPSCs were statistically screened. With this procedure, we can identify 96% of presynaptic cells projecting to the patch-clamped neurons (39). Fig. 1 *E*–*G* shows an example of ROTing-identified synaptic connections, where nine neurons were sequentially whole-cell recorded in pair, and 66 neurons were imaged with fMCI.

In these synapse connection maps, we often found "common" presynaptic neurons that projected to both of the two patched neurons. The mean ratio of common presynaptic neurons to the total presynaptic neurons that projected to at least one of the patched neuron pair was 13.2 ± 2.5%. This proportion increased to 43.9 ± 20.2%, however, when the postsynaptic pairs were synaptically connected (Fig. 1*H*; n = 11 pairs). This suggests that synaptic pairs receive more correlated inputs than nonsynaptic pairs.

To confirm this, we carried out targeted patch-clamp recordings from spontaneously synchronized PC pairs, which were identified online by high-speed fMCI. After monitoring spontaneous spikes in current-clamp mode, sEPSCs and sIPSCs were recorded in voltage-clamp mode at −90 mV and 0 mV, respectively. As expected, these PC pairs received highly correlated sEPSCs and sIPSCs (Fig. 2*A Left*). The cross-correlations peaked sharply at time lags of less than 1 ms (Fig. 2*A Right*). The half peak width in the cross-correlogram was 67.0 ± 56.1 ms for sEPSCs and 54.7 ± 50.4 ms for sIPSCs.

As control experiments, we also targeted less synchronized neuron pairs. In the low-S pairs, sEPSCs were only weakly correlated (Fig. 2*B*), whereas sIPSCs were still highly correlated (Fig. 2*B*). Data are summarized in Fig. 2 *C* and *D*. The correlation coefficients of sEPSCs correlated positively with S (r = 0.34, $P < 0.01$), whereas those of sIPSCs were always high, independent of S. These data imply that excitatory neurons are specifically wired to ensure local synchronization and that inhibitory activity is globally coherent in CA3 networks.

Synchronized Inputs from Common Presynaptic Neurons. How efficiently do common excitatory synaptic inputs produce synchronous firing? With the dynamic-clamp technique, we injected artificially generated "correlated" synaptic conductance patterns into two CA3 PCs under pharmacological blockade of fast synaptic transmission. The stimulus sweeps were constructed *in silico* from spike trains of 200 Poisson-firing presynaptic neurons, in which each spike was convolved with a unitary waveform of a fast excit-

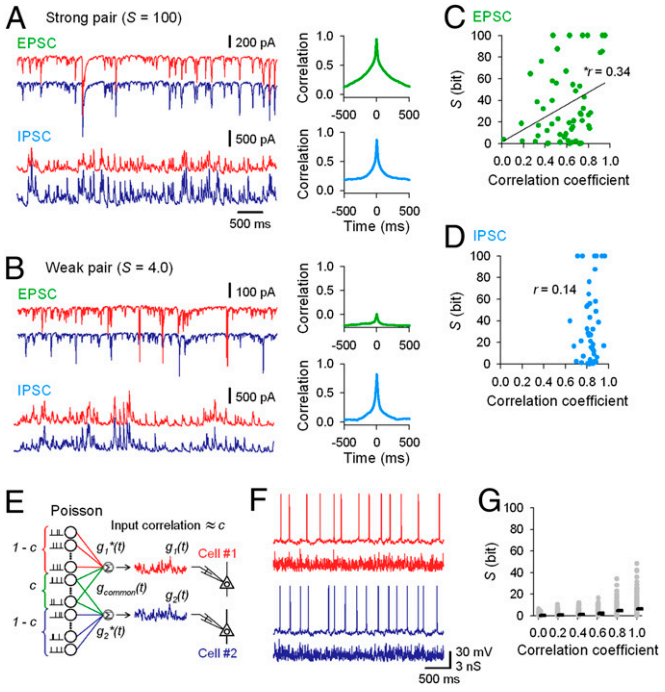

Fig. 2. Correlated sEPSCs in synchronous neuron pairs. (*A*) sEPSCs (*Upper*) and sIPSCs (*Lower*) recorded in a neuron pair with an *S* of 100. Blue and red traces are parts of simultaneous voltage-clamp recordings from two pyramidal neurons. (*B*) In a neuron pair with an *S* of 4.0, sEPSCs were only weakly uncorrelated, but sIPSCs were still strongly correlated. (*C* and *D*) Summary of the relationship between *S* and the correlation coefficient of sEPSCs (*C*) (r = 0.34, P = 0.01; n = 56 pairs) and sIPSCs (*D*) (r = 0.14, $P > 0.1$; n = 55 pairs). (*E*) With the dynamic-clamp technique, correlated excitatory synaptic conductances were injected into two CA3 pyramidal neurons under the pharmacological blockade of fast synaptic transmission. Two stimulation sweeps (red and blue) were generated from partially overlapped Poisson spike trains. (*F*) Spike patterns emitted by two PCs in response to correlated conductance stimuli (correlation coefficient of 0.6). (*G*) *S* was calculated from spike responses and plotted against the correlation coefficients between the injected conductances (n = 55 pairs).

atory postsynaptic conductance. Correlated conductances were generated by overlapping some of the 200 presynaptic spike trains so that their correlation coefficients ranged from 0 to 1 (Fig. 2*E*). When PC pairs were stimulated with these conductances, they emitted spikes, some of which were found to synchronize (Fig. 2*F*). *S* was calculated from the spike series and plotted against the input correlation coefficients. The neurons responded to more correlated inputs with more synchronized spike outputs (Fig. 2*G*). The input-output relationship was substantially weak, however, compared with that observed during spontaneous activity (cf. Fig. 2*C*); note that *S* was always less than 50 bits in the stimulation experiments, whereas it often exceeded 50 bits even for weakly correlated EPSCs in spontaneous activity.

This inconsistency between artificial and spontaneous synaptic inputs suggests that naturally occurring EPSCs involve more information than captured by simple cross-correlations, thereby efficiently synchronizing postsynaptic neurons (40, 41). To seek the underlying information, we examined the dynamics of spontaneous firing activity of CA3 neuron populations. Using high-speed fMCI, the spatiotemporal pattern of spontaneous network activity was reconstructed with the millisecond resolution from 85 ± 25 neurons (n = 14 slices), ranging from 53 to 137 neurons (Fig. 3*A* and Movie S1). Within a given 10-ms period, on average, only a small number of neurons (0.19 ± 0.61% of the total cells; n = 14 slices) were active, whereas the network occasionally exhibited large synchronous events that involved up to approximately 50% neurons (Fig. 3*A Lower*). The frequency of the synchrony sizes was approximated by a power-law distribution $P(n) \approx n^{\alpha}$, where n denotes the synchrony size and $P(n)$ the probability of observing size-n synchrony (Fig. 3*B*; $\alpha = -2.6$). A peri-synchronization time histogram revealed that, in a synchronous event, the network barraged spikes during a period of approximately ±20 ms (Fig. S4). During synchronization, CA1 networks showed high-frequency field oscillations (Fig. S5), which closely resembled sharp-wave/ripples observed in the hippocampus of quiescent or sleeping animals (42).

We computed *S* for all neuron pairs in a raster plot and drew the *S*-based connectivity map (Fig. 3*C*). Synchronization was sparse; *S* was 0 bits in 80.3 ± 17.9% pairs, whereas nonzero *S* conformed to a log-normal Gaussian distribution (Fig. 3*D*). *S* did not correlate with the physical cell-to-cell distance as a whole (r = 0.096, $P > 0.1$), but pairs with $S > 50$ bits were always located within a distance of 200 μm (Fig. 3*E*). Note that closely spaced spikes (>50 Hz firing) were hardly separated in fMCI data (Fig. S6*A*) because Ca^{2+} transients had a long decay constant of approximately 500 ms (43). Therefore, fMCI tends to underestimate *S*, whereas *S* obtained by fMCI was almost linear with electrophysiologically obtained *S* (r = 0.77, $P < 0.01$; Fig. S6*B*).

After constructing the *S* maps, we conducted ROTing in the same network to search common presynaptic neurons. The common presynaptic pairs exhibited significantly higher *S* than unshared pairs (Fig. 3*F*; $P < 0.01$, Kolmogorov-Smirnov test). This suggests that common parents are more prone to synchronize. In other words, inputs into common postsynaptic pairs will be more correlated than "Poisson-correlated" inputs, which we used in the dynamic-clamp experiments (Fig. 2*E*).

Given that network synchronization magnitudes were power-law tailed, we now generated the synaptic conductance patterns from power law-scaled presynaptic spike trains by keeping the overall presynaptic firing rate the same as in the Poisson simulation (Fig. 3*G*). Neuron pairs stimulated by the scaled pattern conductances exhibited strongly synchronized spikes, sometimes reaching an *S* of 100 bits (Fig. 3 *H* and *I*).

Ensemble Dynamics of Spontaneous Activity. Based on the matrices of *S* obtained by fMCI, we constructed dendrograms using the method of Ward, a hierarchical clustering algorithm (Fig. S7*A*). It disclosed the "cliqueness" of synchronous neurons. We then examined whether the *S* matrices included small-world attributes (27). By setting various lower-limit thresholds on the *S* matrices, we depicted the synchrony graphs as a function of the threshold (Fig. S7*B*). For any threshold, the extracted graph exhibited the "small-worldness" (Fig. S7 *C–E*).

Using the affinity propagation algorithm (44), the order of neurons was sorted so that higher *S* pairs were more neighbored in the matrix, and the renumbered neurons were clustered into subgroups. In the representative data shown in Fig. 4*A*, 96 neurons were separated into 15 groups. On average, each movie contained 16.1 ± 7.6 groups, and each group comprised 5.8 ± 4.1 neurons (n = 14 slices). This clustering was validated with ROTing; the connection probability among within-group neurons was 37.6 ± 17.8%, significantly higher than the across-group connectivity (27.0 ± 8.6%, P = 0.04, Wilcoxon signed-rank test; n = 5 slices; Fig. 4*B*).

Neurons within a group were sparsely distributed over the imaged field (Fig. 4*C*). The distribution of the cell-to-cell distance between within-group neurons did not differ from that of across-group neurons (Fig. 4*D*; $P > 0.1$, Kolmogorov-Smirnov test; n = 14 slices), indicating no spatial bias of synchronous spike patterns. Raster plots sorted along the groups demonstrated that within-group neurons frequently exhibited synchronized spikes (Fig. 4*E Upper*). Interestingly, the internal structure of synchronization was dynamic, that is, different synchrony events recruited different sets of neuron groups (Fig. 4*E Lower*).

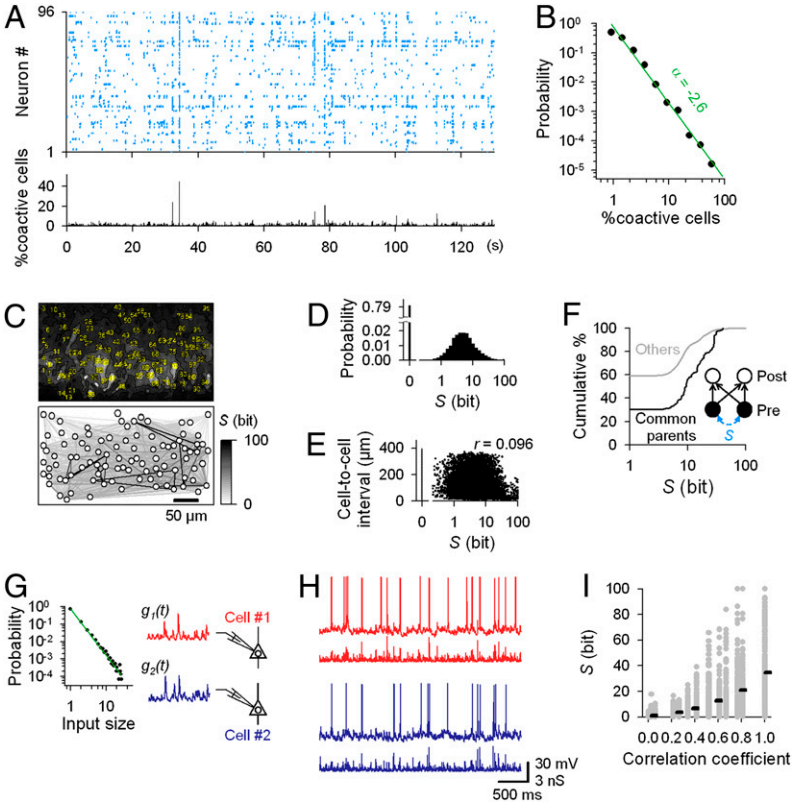

Fig. 3. Heavy-tailed synchronization in spontaneously active networks. (*A*) Rastergram of spontaneous spikes in 96 neurons monitored by high-speed fMCI (*Upper*). Time histogram of the percentage of coactivated cells to the total imaged neurons (*Lower*, 10-ms bin). (*B*) Power-law distributions in synchrony size ($n = 14$ slices). (*C*) Anatomical distribution of 96 neurons imaged in *A* (*Upper*). To quantify the degree of pairwise synchronization, *S* was defined as a surprise index of the probability that the observed number of synchronized spikes could occur under the Poisson process. Gray-scaled *S* between all pairs of 96 cells was shown on the cell map (*Lower*). (*D*) Distribution of *S* (54,239 cell pairs from 14 slices). (*E*) Relationship between *S* and the physical distance between two neurons ($r = 0.096$, $P > 0.1$). (*F*) Pairs of common presynaptic cells shared by any postsynaptic pairs exhibited higher *S* than the others ($P < 0.01$, Kolmogorov-Smirnov test). (*G*) Stimulation sweeps were generated from power law–distributed spike trains. (*H*) Spike patterns in response to power law–scaled conductance stimuli (correlation coefficient of 0.6). (*I*) *S* was plotted against the correlation coefficients of the scaled conductances ($n = 66$ pairs).

Information Flow from CA3 to CA1. Finally, we addressed how these CA3 cell assembly activities are transferred to downstream CA1 networks. After sorting CA3 neurons based on *S* matrices, we applied ROTing to probe the CA3-to-CA1 synaptic connectivity. An example map is presented in Fig. 5*A*, which shows the projection pattern from 90 CA3 neurons to seven patch-clamped

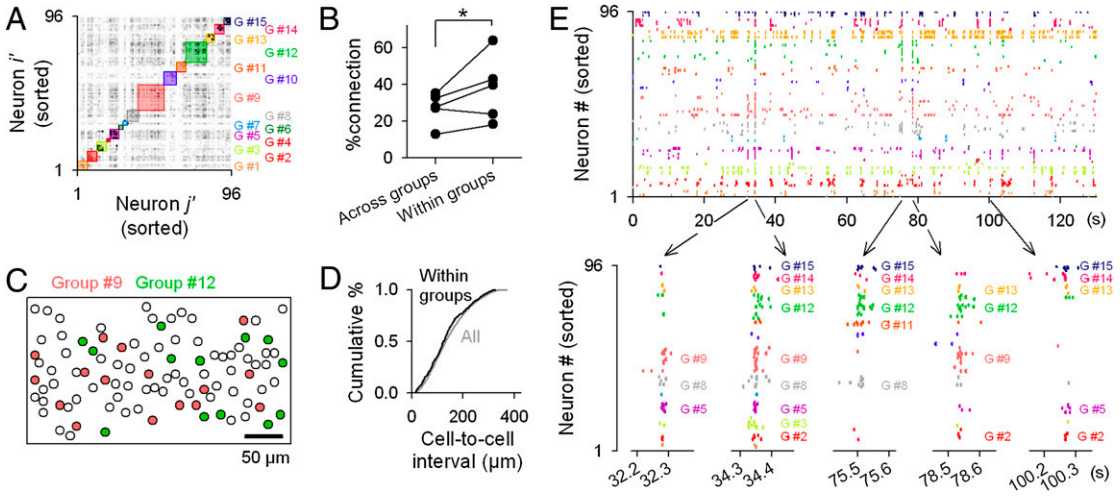

Fig. 4. Cell assembly dynamics in network synchrony. (*A*) Affinity propagation algorithm separated 96 neurons in Fig. 3*A* into 15 subgroups. Each color indicates a single group. (*B*) ROTing was conducted after neuronal group classification. Connection probability is significantly higher for within-group pairs than across-group pairs ($P = 0.04$, Wilcoxon signed-rank test; $n = 5$ slices). (*C*) Cell map of two representative groups found in *A*. (*D*) No significant difference in cumulative distribution of the cell-to-cell distances between within-group pairs (black line) and across-group pairs (gray line; $n = 14$ slices). (*E*) Raster plot (Fig. 3*A*) was sorted in the order of the groups defined in *A*. Five synchrony events are time-expanded (*Lower*). Different events consisted of different group sets.

CA1 PCs. CA3 PC pairs that projected convergently to the same CA1 PCs had statistically higher *S* than the other CA3 PC pairs (Fig. 5*B*; $P < 0.01$, Kolmogorov-Smirnov test). Thus, synchronous CA3 activity tends to converge on the same CA1 neurons.

Discussion

In this study, we used high-speed fMCI to capture the fine-scale structure of spontaneous CA3 network activity and analyzed the organization and generation of spike synchronization with the aid of large-scale optical mapping and dynamic-clamp techniques. We found that complex recruitments of highly synchronized cell assemblies constitute large-scale network synchronization and that the assemblies emerge through presynaptic synchronization.

Origin of Synchronization. More synchronized neuron pairs were more likely to be synaptically linked. We do not think, however, that this synaptic link is enough to synchronize these neurons, because a single synapse is too weak to depolarize beyond the spike threshold. Rather, correlated synaptic inputs from multiple common presynaptic neurons (30–33, 45) are more plausibly causal of spike synchronization. Two lines of evidence are in favor of this hypothesis. First, ROTing revealed that synaptically coupled CA3 PC pairs shared numerically more presynaptic CA3 PCs. Second, double whole-cell recordings of neuron pairs revealed that more synchronized pairs received more correlated sEPSCs.

We also found that common parent PCs were strongly synchronized. This indicates that these common parents are also under the further-upstream innervation by common "grandparent" PCs. This suggests synchronous activity flow, that is, synchronous pulse packets flow across densely connected neuron groups in recurrent networks. This idea is supported by our dynamic clamp data showing that common presynaptic neurons need to be synchronized to evoke a realistic level of postsynaptic synchronization, although common inputs from randomly spiking neurons can do neurons to some extent.

In the dynamic clamp experiments, however, we did not consider the dendritic properties. Dendrites exhibit nonlinear excitation through spatiotemporal input summation and dendritic spikes. It is also possible that synchronized spikes result from nonlinear dendritic computation with convergent inputs of synchronous activity into specific dendritic branches. Research into this possibility is under way in our laboratory with multiple patch-clamp recordings targeting dendrites (46).

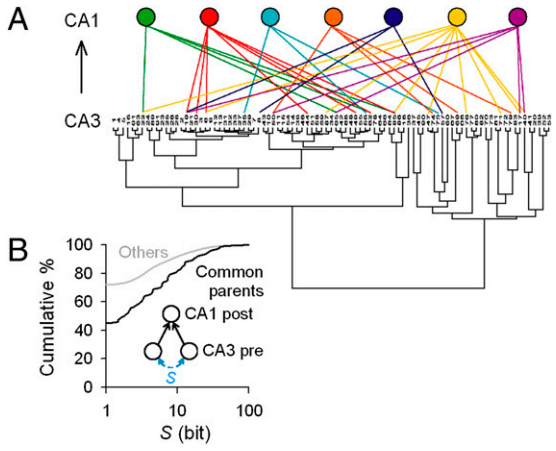

Fig. 5. Convergent projection from synchronized CA3 pairs to CA1 neurons. (*A*) Representative wiring patterns between 91 CA3 and 7 CA1 neurons. For illustration purpose, CA3 neurons were classified on their *S* matrix with the Ward method. (*B*) CA3 neuron pairs that projected convergently to the same CA1 neurons displayed significantly higher *S* than the others ($P < 0.01$, Kolmogorov-Smirnov test; $n = 4$ slices).

Cell Assemblies in Small-World Networks. Consistent with previous reports showing that the functional and anatomical connectivity among individual neurons exhibits small-world architectures (26, 27, 47, 48), the CA3 networks also included small-world topology. The small-world network is theoretically believed to allow fast information transfer with low wiring costs (49), the coexistence of information segregation and integration (50), and synchronization (51). Neurons within a small-world cluster, classified by affinity propagation, were sparsely distributed in space. In hippocampal place cell activity recorded by multiple unit electrodes in vivo, it is also reported that synchronous cliques are dispersed across the electrodes (17). Despite this apparent randomness of neuron locations, within-group neurons were preferentially interconnected. This may emerge from target-selection mechanisms, such as activity-dependent synaptic plasticity. Moreover, synchronous CA3 neuron groups converged onto the same CA1 neurons. Thus, the CA3-to-CA1 connectivity forms relatively independent routes that carry CA3 ensemble activities to specific CA1 neuron subsets (Fig. S8). Synchronous modules may serve as endogenous building blocks that embody the diversity and complexity of information processing in associative and parallel networks.

Coherent Inhibitory Networks. In the rat neocortex, the axons of inhibitory neurons highly arborize, twisting and turning, seemingly rummaging among their postsynaptic targets (52). Therefore, single interneurons may promiscuously provide nearby PCs with correlated inhibitory inputs. Moreover, interneurons are reciprocally connected through synaptic contacts and gap junction (53–55). Thus, their interplay may give rise to globally coherent inhibition of PC networks (56). Indeed we found that sIPSCs were correlated between virtually all PC pairs. Inhibitory inputs limit the window available for temporal summation and increase the temporal precision of PC firing (57). They also entrain network activity by interacting with intrinsic oscillatory mechanisms of PCs (58). We thus speculate that interneurons couple relatively independent PC subgroups and orchestrate complex network synchronization.

Ex Vivo Data. Our data were obtained exclusively from organotypic slice cultures, an ex vivo experimental network model, and hence must be carefully extrapolated to other neuronal systems, such mature brain networks in vivo. Nonetheless, it is still intriguing to find that such spontaneously reorganized ex vivo networks show highly nonrandom patterns of connectivity and activity. Our findings thus describe a primary regime of how neuronal networks intrinsically develop and operate in the "free-run" mode.

Materials and Methods

Experiments were performed with the approval of the animal experiment ethics committee at the University of Tokyo (approval number 19-43, A21-6) according to the University of Tokyo guidelines for the care and use of laboratory animals.

Entorhino-hippocampal organotypic slices were prepared from 7-d-old Wistar/ST rats (SLC). Experiments were performed on days 7 to 11 in vitro. Patch-clamp recordings were carried out simultaneously from two to four PCs with two Axopatch 700B dual amplifiers (Molecular Devices). Whole-cell patch pipettes (4–6 MΩ) were filled with 135 mM K-gluconate, 4 mM KCl, 10 mM Hepes, 10 mM phosphocreatine, 4 mM MgATP, 0.3 mM NaGTP, and 0.2% biocytin. Dynamic-clamp stimulation was performed with a PCI-6024E data acquisition board (National Instruments) under a real-time Linux-environment.

For fMCI, slices were incubated with Oregon Green 488 BAPTA-1 AM at 37 °C for 1 h and imaged at 500 to 2,000 frames per s with a Nipkow-disk confocal unit (CSUX-1; Yokogawa Electric), a high-speed back-illuminated CCD camera (iXon DU860; Andor), and a water-immersion objective lens (magnification ×16, 0.80 NA; Nikon). Spike timings were determined with an automatic machine-learning algorithm. Spike train data used here are available online at http://hippocampus.jp/data. Further details are provided in *SI Materials and Methods*.

ACKNOWLEDGMENTS. We are grateful to Ms. Huei-Yu Chiou (Graduate School of Pharmaceutical Sciences, University of Tokyo) for providing us with in vivo whole-cell recording data. This work was supported in part by a Grant-in-Aid for Science Research on Priority Areas (Elucidation of neural network function in the brain, 18021008, 17023015, and 20019014); a Grant-in-Aid for Science Research (17650090, 17689004, and 19659013) from the Ministry of Education, Culture, Sports, Science, and Technology of Japan; and Sumitomo Foundation Grant 050038.

1. Engel AK, Fries P, Singer W (2001) Dynamic predictions: Oscillations and synchrony in top-down processing. *Nat Rev Neurosci* 2:704–716.
2. Salinas E, Sejnowski TJ (2001) Correlated neuronal activity and the flow of neural information. *Nat Rev Neurosci* 2:539–550.
3. Zohary E, Shadlen MN, Newsome WT (1994) Correlated neuronal discharge rate and its implications for psychophysical performance. *Nature* 370:140–143.
4. Vaadia E, et al. (1995) Dynamics of neuronal interactions in monkey cortex in relation to behavioural events. *Nature* 373:515–518.
5. deCharms RC, Merzenich MM (1996) Primary cortical representation of sounds by the coordination of action-potential timing. *Nature* 381:610–613.
6. Riehle A, Grün S, Diesmann M, Aertsen A (1997) Spike synchronization and rate modulation differentially involved in motor cortical function. *Science* 278:1950–1953.
7. Stopfer M, Bhagavan S, Smith BH, Laurent G (1997) Impaired odour discrimination on desynchronization of odour-encoding neural assemblies. *Nature* 390:70–74.
8. Steinmetz PN, et al. (2000) Attention modulates synchronized neuronal firing in primate somatosensory cortex. *Nature* 404:187–190.
9. Gray CM, Singer W (1989) Stimulus-specific neuronal oscillations in orientation columns of cat visual cortex. *Proc Natl Acad Sci USA* 86:1698–1702.
10. Abeles M (1991) *Corticonics: Neural circuits of the cerebral cortex* (Cambridge Univ Press, Cambridge, UK).
11. Diesmann M, Gewaltig MO, Aertsen A (1999) Stable propagation of synchronous spiking in cortical neural networks. *Nature* 402:529–533.
12. Markram H, Lübke J, Frotscher M, Sakmann B (1997) Regulation of synaptic efficacy by coincidence of postsynaptic APs and EPSPs. *Science* 275:213–215.
13. Bi GQ, Poo MM (1998) Synaptic modifications in cultured hippocampal neurons: dependence on spike timing, synaptic strength, and postsynaptic cell type. *J Neurosci* 18:10464–10472.
14. Hebb DO (1949) *The organization of behavior: A neuropsychological theory* (John Wiley and Sons, New York).
15. Nicolelis MA, Baccala LA, Lin RC, Chapin JK (1995) Sensorimotor encoding by synchronous neural ensemble activity at multiple levels of the somatosensory system. *Science* 268:1353–1358.
16. Laubach M, Wessberg J, Nicolelis MA (2000) Cortical ensemble activity increasingly predicts behaviour outcomes during learning of a motor task. *Nature* 405:567–571.
17. Harris KD, Csicsvari J, Hirase H, Dragoi G, Buzsáki G (2003) Organization of cell assemblies in the hippocampus. *Nature* 424:552–556.
18. Ikegaya Y, et al. (2004) Synfire chains and cortical songs: temporal modules of cortical activity. *Science* 304:559–564.
19. Beggs JM, Plenz D (2003) Neuronal avalanches in neocortical circuits. *J Neurosci* 23: 11167–11177.
20. Schneidman E, Berry MJ, 2nd, Segev R, Bialek W (2006) Weak pairwise correlations imply strongly correlated network states in a neural population. *Nature* 440: 1007–1012.
21. Shlens J, et al. (2006) The structure of multi-neuron firing patterns in primate retina. *J Neurosci* 26:8254–8266.
22. Tang A, et al. (2008) A maximum entropy model applied to spatial and temporal correlations from cortical networks in vitro. *J Neurosci* 28:505–518.
23. Beggs JM, Plenz D (2004) Neuronal avalanches are diverse and precise activity patterns that are stable for many hours in cortical slice cultures. *J Neurosci* 24: 5216–5229.
24. Eytan D, Marom S (2006) Dynamics and effective topology underlying synchronization in networks of cortical neurons. *J Neurosci* 26:8465–8476.
25. Sasaki T, Matsuki N, Ikegaya Y (2007) Metastability of active CA3 networks. *J Neurosci* 27:517–528.
26. Yu S, Huang D, Singer W, Nikolic D (2008) A small world of neuronal synchrony. *Cereb Cortex* 18:2891–2901.
27. Watts DJ, Strogatz SH (1998) Collective dynamics of 'small-world' networks. *Nature* 393:440–442.
28. Holmgren C, Harkany T, Svennenfors B, Zilberter Y (2003) Pyramidal cell communication within local networks in layer 2/3 of rat neocortex. *J Physiol* 551:139–153.
29. Shepherd GMG, Stepanyants A, Bureau I, Chklovskii DB, Svoboda K (2005) Geometric and functional organization of cortical circuits. *Nat Neurosci* 8:782–790.
30. Song S, Sjöström PJ, Reigl M, Nelson S, Chklovskii DB (2005) Highly nonrandom features of synaptic connectivity in local cortical circuits. *PLoS Biol* 3:e68.
31. Yoshimura Y, Dantzker JL, Callaway EM (2005) Excitatory cortical neurons form fine-scale functional networks. *Nature* 433:868–873.
32. Kampa BM, Letzkus JJ, Stuart GJ (2006) Cortical feed-forward networks for binding different streams of sensory information. *Nat Neurosci* 9:1472–1473.
33. Otsuka T, Kawaguchi Y (2008) Firing-pattern-dependent specificity of cortical excitatory feed-forward subnetworks. *J Neurosci* 28:11186–11195.
34. Lefort S, Tomm C, Floyd Sarria JC, Petersen CC (2009) The excitatory neuronal network of the C2 barrel column in mouse primar somatosensory cortex. *Neuron* 61:301–316.
35. Miles R, Wong RK (1986) Excitatory synaptic interactions between CA3 neurones in the guinea-pig hippocampus. *J Physiol* 373:397–418.
36. Smith KL, Szarowski DH, Turner JN, Swann JW (1995) Diverse neuronal populations mediate local circuit excitation in area CA3 of developing hippocampus. *J Neurophysiol* 74:650–672.
37. Gomez-Di Cesare CM, Smith KL, Rice FL, Swann JW (1997) Axonal remodeling during postnatal maturation of CA3 hippocampal pyramidal neurons. *J Comp Neurol* 384: 165–180.
38. Weaver W (1948) Probability, rarity, interest, and surprise. *Sci Mon* 67:390–392.
39. Sasaki T, Minamisawa G, Takahashi N, Matsuki N, Ikegaya Y (2009) Reverse optical trawling for synaptic connections in situ. *J Neurophysiol* 102:636–643.
40. Stevens CF, Zador AM (1998) Input synchrony and the irregular firing of cortical neurons. *Nat Neurosci* 1:210–217.
41. DeWeese MR, Zador AM (2006) Non-Gaussian membrane potential dynamics imply sparse, synchronous activity in auditory cortex. *J Neurosci* 26:12206–12218.
42. Buzsáki G (1989) Two-stage model of memory trace formation: A role for "noisy" brain states. *Neuroscience* 3:551–570.
43. Sasaki T, Takahashi N, Matsuki N, Ikegaya Y (2008) Fast and accurate detection of action potentials from somatic calcium fluctuations. *J Neurophysiol* 100:1668–1676.
44. Frey BJ, Dueck D (2007) Clustering by passing messages between data points. *Science* 315:972–976.
45. Kazama H, Wilson RI (2009) Origins of correlated activity in an olfactory circuit. *Nat Neurosci* 12:1136–1144.
46. Ishikawa D, et al. (2010) Fluorescent pipettes for optically targeted patch-clamp recordings. *Neural Netw*, in press.
47. Bettencourt LM, Stephens GJ, Ham MI, Gross GW (2007) Functional structure of cortical neuronal networks grown in vitro. *Phys Rev E Stat Nonlin Soft Matter Phys* 75: 021915.
48. Pajevic S, Plenz D (2009) Efficient network reconstruction from dynamical cascades identifies small-world topology of neuronal avalanches. *PLOS Comput Biol* 5: e1000271.
49. Buzsáki G, Geisler C, Henze DA, Wang XJ (2004) Interneuron Diversity series: Circuit complexity and axon wiring economy of cortical interneurons. *Trends Neurosci* 27: 186–193.
50. Sporns O, Zwi JD (2004) The small world of the cerebral cortex. *Neuroinformatics* 2: 145–162.
51. Barahona M, Pecora LM (2002) Synchronization in small-world systems. *Phys Rev Lett* 89:054101.
52. Stepanyants A, Tamás G, Chklovskii DB (2004) Class-specific features of neuronal wiring. *Neuron* 43:251–259.
53. Fukuda T, Kosaka T (2000) Gap junctions linking the dendritic network of GABAergic interneurons in the hippocampus. *J Neurosci* 20:1519–1528.
54. Tamás G, Buhl EH, Lörincz A, Somogyi P (2000) Proximally targeted GABAergic synapses and gap junctions synchronize cortical interneurons. *Nat Neurosci* 3: 366–371.
55. Bartos M, et al. (2002) Fast synaptic inhibition promotes synchronized gamma oscillations in hippocampal interneuron networks. *Proc Natl Acad Sci USA* 99: 13222–13227.
56. Poo C, Isaacson JS (2009) Odor representations in olfactory cortex: "Sparse" coding, global inhibition, and oscillations. *Neuron* 62:850–861.
57. Pouille F, Scanziani M (2001) Enforcement of temporal fidelity in pyramidal cells by somatic feed-forward inhibition. *Science* 293:1159–1163.
58. Cobb SR, Buhl EH, Halasy K, Paulsen O, Somogyi P (1995) Synchronization of neuronal activity in hippocampus by individual GABAergic interneurons. *Nature* 378:75–78.